COMPARISON OF COMPACT POLARIMETRIC WITH FULL POLARIMETRIC RADAR DATA FOR LAND USE DISCRIMINATION BASED ON SVM CLASSIFICATION

C. Lardeux[(1)], P.-L. Frison [(1)], C. Tison[(2)], D. Deleflie, J.-C. Souyris[(2)], J.-P. Rudant[(1)], B. Stoll[(3)]

[(1)]Université de Marne la Vallée, laboratoire G2I-IFSA, 5 boulevard Descrates, 77 454 Marne la Vallée Cedex 2
Email: cedric.lardeux@univ-mlv.fr
[(2)]Centre National d'Etudes Spatiales, DCT/SI/AR, 18 avenue Edouard Belin, 31 401 Toulouse Cedex 4, France
Email: celine.tison@cnes.fr
[(3)]Université de Polynésie Française, B.P. 6570 98702 FAA'A Aeroport Tahiti - Polynésie Française
Email : benoit.stoll@upf.fr

ABSTRACT

This study comes within the framework of the global cartography and inventory of the Polynesian landscape. An AIRSAR airborne acquired fully polarimetric data in L band, in August 2000, over the main Polynesian Islands. This study focuses on Tubuai Island, where several ground surveys allow the validation of the different results. While they preserve some of the polarimetric information as those that would be recorded by a full polarimetric (FP) radar sensor, compact polarimetry architectures are relevant for systems constraints reduction. Focus is put on the *"π/4"* mode that is simulated from FP data. It has been shown that this mode is particularly efficient for applications dealing with distributed targets like land use classification. In this study, the SVM (Support Vector Machine) algorithm is used as classification method due to its ability to handle linearly non separable cases by using the kernel method. In particular, it is well suited for combining numerous heterogeneous indicators such as intensity channels, polarimetric descriptors, or textural parameters.
The results show that for full polarimetric data, the SVM classification performance when only the elements of the polarimetric coherence matrix are involved is comparable to the Wishart classification one. The addition of polarimetric indices improves significantly the classification. On the other hand when *"π/4"* mode is simulated, the overall classification performance is similar (κ lower of 3%) than those observed with full polarimetric data, with a higher confusion for the *Pinus* class. Moreover, the *"π/4"* mode shows much better performance for the land use discrimination of the studied scene than ENVISAT Alternate Polarisation modes involving intensities acquired in co or cross polarization.

1. INTRODUCTION

Radar data are of particular interest over tropical areas such as the French Polynesian Islands because of persistent cloudy weather. Fully polarimetric SAR data were acquired in L and P bands over the main Polynesian islands. The overall goal of this study is to assess the potential of such fully polarimetric SAR data and to test in the same way the *"π/4"* mode [1] for land-use cartography. When dealing with classification methods applied to full polarimetric data, the Wishart classification [2] is generally used. It may also relies on polarimetric decomposition such as the H/A/α decomposition [3]. In order to integrate heterogeneous polarimetric descriptors (*i.e.* not only the coherence matrix used in the Wishart classification, but also other polarimetric descriptors, such the H/A/α parameters), it is proposed to use the SVM (Support Vector Machine) classification method [4]. It is especially well suited to handle linearly non separable case by using Kernel functions. It has been mostly applied to hyperspectral remote sensed data and few studies have also been conducted with SAR data [5] [6]. The study area and radar data are presented in the second part of this paper. The third part presents the polarimetric indices used in the feature vector, describes shortly the π/4 mode [1], and briefly exposes the principle of the SVM method. The results are presented in the last part of the paper.

2. STUDY AREA AND DATASET

2.1. Study area

French Polynesia islands are located at the middle of the South Pacific Ocean. They are quickly evolving in the tourism industry, and from the economic and geostrategic points of view. They are thus subject to a strong environmental planning leading to landscape changes as well as to the introduction of invasive species. This study comes within the framework of the global cartography and inventory of the Polynesian landscape. We focus on data acquired over the Tubuai Island, in the Australes Archipelago at the South of French Polynesia. Tubuai is a 45 km^2 island with a population of about 6000 inhabitants. It is particularly relevant because of its great landscape diversity: several types of forests, agricultural fields, and residential areas. The objective is to estimate different land use class, in particular by discriminating different forest types containing four classes: *Hibiscus tiliaceus* (also called

Purau), *Pinus Caribeae* (also called Pinus), *Paraserianthes Falcataria* (also called Falcata). The 2 other classes are the one labelled "Low Vegetation", including fern lands, swamps vegetation, and few crops and the "Other" class including bare fields, low grass fields, and urban areas. Several ground surveys has been carried out, and a Quikbird image acquired in August 2004 is also available to supply an accurate validation data set over the entire island.

Figure 1. Tubuai Island : Quickbird (true colors)

The class are summarized in Table 1 with the number of pixels of the radar image associated to training and control classes.

Table 1: Training and testing samples number used for the Tubuai Island classification

Class	Training samples	Control samples
Pinus	5330	5330
Falcata	2696	2696
Purau	6202	6202
Low Vegetation	7897	7897
Other	4457	4457

2.2. Airsar data

An AIRSAR airborne mission took place in August 2000 over the main Polynesian islands. The AIRSAR data were acquired over Tubuai along 2 passes in reverse path, in Polsar mode. The data set used in this study consists in full polarimetric data in L (□ = 23 cm) and P (□ = 67cm) bands with an additional C band channel (□=5.7cm) in VV polarization. Full polarimetric data are delivered in MLC (Multi Look Complex) format, corresponding to about 9 looks, with a resolution of 5 meters. The relative phase of the original data has been calibrated following [7] and an intensity bias has been corrected both in L and P bands values. An AIRSAR composite image is presented on Figure 2.

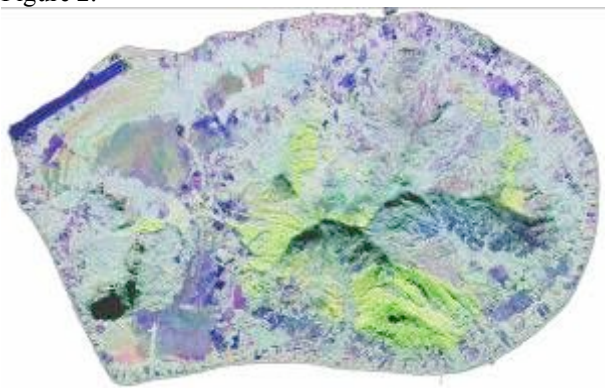

Figure 2. Tubuai Airsar composite (R :L_{HH}, G :P_{HV}, B :C_{VV})

3. Methodology

3.1. Support Vector Machine

A brief description of SVM is made below and more details can be found in [4].

- **Linear case** :

Let us consider a two class classification problem with N training samples. Each sample is described by a Support Vector (SV) X_i composed by the different "bands" with n dimension. The label of a sample is Y_i. For a two classes case we consider the label -1 for the first class and +1 for the other.

The SVM model ω describes the optimal hyperplane which separate the two classes (Figure 3). The classification function f is consequently defines as $f(x) = \text{sign}(\langle \grave{u}, X \rangle + b)$

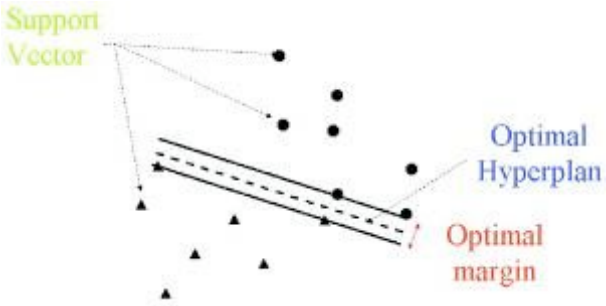

Figure 3. SVM Classifier-Linear case

The sign of f(x) gives the label of the sample. The goal of the SVM is to maximize the margin between the optimal hyperplane and the support vector. So we search for the $\min(\frac{\|\omega\|}{2})$.To do this, it is more easier to use the Lagrange multiplier. The problem comes to solve:

$$f(x) = Sign(\sum_{i=1}^{Ns} y_i.\alpha_i.\langle x, x_i \rangle + b) \quad (1)$$

Where α_i is the Lagrange multiplier.

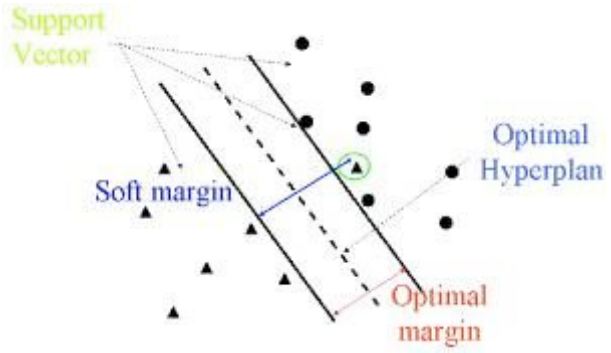

Figure 4. SVM Classifier-Nonlinear case

Soft margin enables to get robust to noisy training data set.

λ **Nonlinear case :**

When classification problem is not linear (Figure 4) the training vectors are projected into a "feature space" H of higher dimension through the feature function Φ ($\Phi : \Re^n \rightarrow H$). In H, the data become linearly separable. Actually, in SVM model, the function Φ is replaced by its scalar product, the Kernel function: $K(x, x_i) = \langle \Phi(x), \Phi(x_i) \rangle$. Then the new classification function is equal to:

$$f(x) = Sign(\sum_{i=1}^{Ns} y_i.\alpha_i.K(x, x_i) + b) \quad (2)$$

Three kernels are commonly used:

- The polynomial kernel $K(x, x_i) = (\langle x, x_i \rangle + 1)^p$
- The sigmoid kernel $K(x, x_i) = \tanh(\langle x, x_i \rangle + 1)$
- The RBF kernel $K(x, x_i) = \exp - \frac{|x - x_i|^2}{2\sigma^2}$

The RBF kernel has been selected in this work through empirical considerations. A future work would be to develop a new kernel accounting for the distribution of the data, such the one is due to the presence of speckle in SAR data.

- Multiclass case :

The principle of SVM has been developed for a two class problem but it has been easily extended to a multi-class problem with several algorithms. Among them, there are:

the "One Against All" (OAA) and the "One Against One" (OAO) algorithms.

If we consider a problem with K class:
The OAA algorithm consists in the construction of k hyperplane that separate respectively one class and the (k-1) other classes.
The OAO algorithm consists in the construction of $\frac{k(k-1)}{2}$ hyperplane which separate each pair of classes.
In the two cases the final label is that mainly chosen. After several tests, the OAO algorithm has been retained as well as the RBF kernel with σ=0.5 and the cost parameter equal to 1000 (soft margin).
The Libsvm library has been used [8].

3.2. Polarimetric indices

Several Support Vectors have been defined for full polarimetric data to measure the impact of the different polarimetric indicators. On the one hand a support vector (referenced *SV1* hereafter) is made up by the 9 elements only of the coherency matrix T. This latter is constructed from the scattering vector k_p expressed in the Pauli basis as follows:

$$k_p = \frac{1}{\sqrt{2}} \begin{pmatrix} S_{HH} + S_{VV} \\ S_{HH} - S_{VV} \\ 2.S_{HV} \end{pmatrix}, [T] = k_p.k_p^{*T} \quad (3)$$

S_{wx} denotes the scattering matrix element corresponding to the *w/x* polarization for the receiving/transmitting wave (*w*, *x* referring to horizontal, H, or vertical, V, linear polarization)
On the other hand, a second support vector, *SV2*, is built with the addition of different polarimetric indices. These are detailed hereafter and summarized in Table 2:

- The intensities in the 2 co- and 1 cross- polarized channel in linear and circular polarization:

$$I_{wx} = |S_{wx}|^2 \quad (4)$$

where *w* and *x* refer to H, V, left, L, and/or right, R, circular polarization.

- The Span:

$$SPAN = I_{HH} + 2\,I_{HV} + I_{VV} \quad (5)$$

- The texture is taken into account through the coefficient of variation $c_v = \frac{\sigma}{\mu}$, σ and μ are representing the standard deviation and mean of the intensities in the linear and circular polarization (3) computed over a 5x5 neighbourhood.
- The ratio between the following intensities:

$$\frac{I_{HV}}{I_{HH}}, \frac{I_{HV}}{I_{VV}}, \frac{I_{HH}}{I_{VV}}, \frac{I_{LL}}{I_{LR}} \quad (6)$$

Table 2: Support Vector configuration

SV1	# el^{ts}	SV2	# el^{ts}
T elements	9	T elements	9
		I_{HH}, I_{HV}, I_{VV}, I_{LL}, I_{LR}, I_{RR}	6
		$SPAN = \lvert S_{HH}\rvert^2 + 2\lvert S_{HV}\rvert^2 + \lvert S_{VV}\rvert^2$	1
		$c_{v\text{-}HH}$, $c_{v\text{-}HV}$, $c_{v\text{-}VV}$, $c_{v\text{-}LL}$, $c_{v\text{-}RR}$, $c_{v\text{-}LR}$,	6
		$\frac{I_{HV}}{I_{HH}}, \frac{I_{HV}}{I_{VV}}, \frac{I_{HH}}{I_{VV}}, \frac{I_{LL}}{I_{LR}}$	4
		$\lvert\tilde{n}_{ÇH-VV}\rvert, \lvert\tilde{n}_{HV-VV}\rvert, \lvert\tilde{n}_{HV-HH}\rvert$ $\lvert\tilde{n}_{LL-LR}\rvert, \lvert\tilde{n}_{RR-LR}\rvert, \lvert\tilde{n}_{LL-RR}\rvert$	6
		P_{min}	1
		Deg_{min}	1
		m and γ Euler parameters :	2
		H/A/α	3
Total	9		39

- The modulus of the degree of coherence, $\lvert\tilde{n}_{ÇH-VV}\rvert, \lvert\tilde{n}_{ÇV-VV}\rvert, \lvert\tilde{n}_{ÇV-HH}\rvert, \lvert\tilde{n}_{LL-LR}\rvert, \lvert\tilde{n}_{RR-LR}\rvert, \lvert\tilde{n}_{LL-RR}\rvert$ computed as follow:

$$\lvert\rho_{wxyz}\rvert = \left| \frac{\langle S_{wx}.S_{yz}^{*}\rangle}{\sqrt{\langle\lvert S_{wx}\rvert^2\rangle.\langle\lvert S_{yz}\rvert^2\rangle}} \right| \quad (7)$$

where w, x, y, z, stands for H, V, L and R polarization

- The minimum power of the backscattered wave, P_{min}, for all the polarization configuration of the emitted wave.
- The minimum of the degree of polarization of the received wave $\partial P_{\min}$ for all the polarization configurations of the emitted wave. The degree of polarization is defined as

$$\partial P = \frac{\sqrt{S_2^2 + S_3^2 + S_4^2}}{S_1} \quad (8)$$

S_1, S_2, S_3, S_4 being the 4 elements of the Stokes vector.

- The 2 Euler parameters m and γ representing respectively the magnitude and the polarisability of the resolution cell. Details about their calculation from the Stokes parameters are given in [9].
- The 3 parameters $H/A/\alpha$ representing the entropy, the scattering mechanism, and the anisotropy [3])

The polarimetric filter developed by Lee [10] has been applied to the full polarimetric data. Then different polarimetric indices has been calculated at the exception of the coefficient of variation that is computed on a 5 x 5 neighborhood of the original data.

3.3. Compact Polarimetry: the *"π/4"* Mode

The *"π/4"* mode consists in a transmitter polarization either circular or oriented at 45°, and in receivers that are in horizontal and vertical polarizations with respect to the line of sight.

Due to some symmetry properties (reflection, rotation, azimuthal) for natural media, some hypothesis could be made to reconstruct the full polarimetric information. More details are given in [1] but one important property used to reconstruct the full polarimetric information is:

$$\left\langle S_{HH}.S_{HV}^{*}\right\rangle = \left\langle S_{HV}.S_{VV}^{*}\right\rangle = 0 \quad (8)$$

This property is generally observed over vegetated areas.

Consequently, some polarimetric parameters loose their signification or become redundant with other. For example, the circular intensities I_{LL} and I_{RR}.are equal. In the same way, the degree of coherence ρ_{llrr} has no more interest, as well as the degree of coherence involving the cross linear polarisation HV that is equal to zero. The primitives defining the Support Vector SVp2, similar to SV2 for the "*π/4*" mode is summarized in Table 3.

Table 3: Support Vector configuration

SVp2	# el^{ts}
T elements	7
I_{HH}, I_{HV}, I_{VV}, I_{LL}, I_{LR}	5
$SPAN = \lvert S_{HH}\rvert^2 + 2\lvert S_{HV}\rvert^2 + \lvert S_{VV}\rvert^2$	1
$c_{v\text{-}HH}$, $c_{v\text{-}HV}$, $c_{v\text{-}VV}$, $c_{v\text{-}LL}$, $c_{v\text{-}RR}$, $c_{v\text{-}LR}$,	6
$\frac{I_{HV}}{I_{HH}}, \frac{I_{HV}}{I_{VV}}, \frac{I_{HH}}{I_{VV}}, \frac{I_{LL}}{I_{LR}}$	4
$\lvert\tilde{n}_{ÇH-VV}\rvert, \lvert\tilde{n}_{LL-LR}\rvert$	2
P_{min}	1
Deg_{min}	1
m and γ Euler parameters :	2
H/A/α	3
Total number of primitives	32

4. Results and discussion

4.1.1. Full Polarimetric data

In order to assess the suitability of the SVM algorithm to polarimetric SAR data, the SVM with the SV1 support vector has been compared to the Wishart classification [2] over an extract.

The overall performance of the classification is given by the Kappa coefficient, κ, while the Producer Accuracy is used to estimate the performance for the different classes [12].

Both classifications show the same performance with the same Kappa coefficient, for Wishart and SVM algorithms. The values obtained are κ = 50 % and κ = 56 % for the L and P bad respectively. It can be noticed that a high confusion is observed for the different forest types for both bands.

In a second step, the SV2 Support Vector has been used in order to assess the contribution of the polarimetric indices. Results are presented in Table 4.
The polarimetric indices have a significant contribution in the SVM classification as, with the SV2 Support Vector, κ= *72* % and κ= *74* % for L and P band. These values show a significant improvement as they have to be compared with those obtained with SV1 Support Vector over the whole scene, giving κ= *64* % and κ= *67* % for L and P band respectively. Both bands present again the same performance with still significant confusion between the different forest types.
When the L and P bands are combined, leading to a Support vector of 78 components, there is an increase of 5% for the κ value that reaches 79%. The *Pinus* forest type is much better discriminated (PA = 83 %) while the *Purau* and the *Falcata* present still high confusion. Finally, the addition of the C band-VV polarisation intensity data (leading to a 79 components Support Vector) is of significant added-value as κ = 86%. In particular, it increases significantly the *Purau* discrimination, while there is still persistent confusion concerning *Falcata*.

Table 4: SVM classification results with SV2: the Producer Accuracy (%) is given for the different classes, and the overall performance is given by κ

	L	P	L+P	L+P+C_{VV}
Pinus	61	67	83	98
Falcata	48	46	47	56
Purau	67	75	81	90
Low Vegetation	97	96	97	98
Other	93	90	91	91
κ *(%)*	72	74	79	86

4.1.2. π/4 configuration

Results obtained in L band for the *"π/4"* mode with the SVp2 Support Vector (cf. Table 3) are given in Table 5. By comparison with the first column of Table 4, the overall performance (κ = 69 %) is similar to the classification involving full polarimetric data as a difference of only 3% is observed. With regards to the different land use classes, the biggest difference is observed for the *Falata* with a producer accuracy equal to 39 %, *i. e.* 9 % lower than for the full polarimetric data. Quite similar results are observed over the other land classes.

Table 5: SVM classification results with SVp2: the Producer Accuracy (%) is given for the different classes, and the overall performance is given by κ *(%).*

Pinus	*Falcata*	*Purau*	*Low vegetation*	*Other*	κ
57	39	66	94	89	69

For comparison, the overall performance obtained with 3 mono polarization channel in P_{HV}, L_{HH}, and C_{VV} configuration is quite comparable with κ = 74 %. Moreover, simulations of ENVISAT Alternate Polarization mode in L band, give κ = 53 % and κ = 57 % for HH/VV and HH/HV respectively. The classification obtained with intensities acquired with HH/HV/VV polarisation (as that would be obtained with 2 passes of ENVISAT in Alternate Polarisation) does not increases significantly the overall performance with κ = 59 %. These results, summarized in Table 6, show the significant advantage of the *"π/4"* mode towards AP mode for classification of such landscapes.

Table 6: Overall classification results obtained from different compact architecture configuration in L band

	Full polar	*π/4*	*HH/VV*	*HH/HV*	*HH/HV/VV*
κ *(%)*	72	69	53	57	59

5. Conclusion

This study shows that the SVM classification algorithm is well suited for full polarimetric data with similar accuracy as Wishart classification. The possibility to add different polarimetric or textural indices makes the SVM algorithm very interesting as the overall performance giving by the κ value increases of 22%. Moreover, the simulation of compact architecture like the *"π/4"* mode shows comparable results to full polarimetric SVM classification, while results obtained with ENVISAT Alternate Polarization simulations (HH/VV, HH/HV, HH/HV/VV) are of the same order of magnitude than the Wishart classification.

Acknowledgment

The authors are very grateful to Jean-Yves Meyer for for the survey mission and we would like to thank the Government of French Polynesia and its Urbanism Department for providing the AirSAR, MASTER and Quickbird data required for this study.

References

[1] J.-C. Souyris, P. Imbo, R. Fjørtoft, S. Mingot, J.-S. Lee, *Compact Polarimetry Based on Symmetry Properties of Geophysical Media: The π/4 Mode,* IEEE Trans. Geosci. Remote Sens., vol. 43, no. 3, Mar. 2005. Page(s):634 – 646

[2] J. S. Lee, M. R. Grunes, R. Kwok, *Classification of multi-look polarimetric SAR imagery based on complex Wishart distribution,* Int. J. Rem. Sens., vol. 15, n° 11, 1994, 2299-2311.

[3] S. R. Cloude, E. Pottier *A Review of Target Decomposition Theorems in Radar Polarimetry*, IEEE TGRS, vol. 34, no. 2, pp 498-518, Sept. 1995.

[4] C. J. Burges, *A tutorial on support vector machines for pattern recognition*, in Data mining and knowledge discovery, U. Fayyad, Ed. Kluwer Academic, 1998, pp. 1-43.

[5] S. Fukuda and H. Hirosawa *Support Vector Machine Classification of Land Cover: Application to Polarimetric SAR Data* in Geoscience and Remote Sensing Symposium, 2001. IGARSS '01. IEEE 2001 International, 9-13 July 2001 Page(s):187 - 189 vol.1

[6] G. Mercier and F. Girard-Ardhuin, *Unsupervised Oil Slick Detection by SAR Imagery using Kernel Expansion*, Geoscience and Remote Sensing Symposium, 2005. IGARSS '05. Proceedings. 2005 IEEE International vol.1, 25-29 July 2005 Page(s):494 – 497

[7] H. A. Zebker, J. J. van Zyl, and D.H.Held, *Imaging radar polarimetry frow waves synthesis*, J.Geophy. Res, vol. 91, no B5. pp. 683-701, Jan. 1987.

[8] Libsvm is available at http://www.csie.ntu.edu.tw/cjlin/libsvm

[9] D. Laurent, E. Pottier, and J. Saillard *The Euler vector : a polarimetric descriptor of the ocean surface*, journal of Electromagnetic Waves and Applications. vol. 9, n1/2 pp 217-240, 1995

[10] J. S. Lee, M. R Grunes, G. de Grandi,, *Polarimetric SAR speckle filtering and its implication for classification*, IEEE Trans. Geosci. and Rem. Sens., vol. 37, n0 5, 1999, 2362-2373

[11] ESA,*PolSarPro*, available at http://earth.esa.int/polsarpro/

[12] T. M. Lillesand and R. W. Kiefer, *Remote sensing and Image interpretation*, 3rd ed., New York: Wiley, 1993.